HHS Public Access

Author manuscript

Angew Chem Int Ed Engl. Author manuscript; available in PMC 2023 February 21.

Published in final edited form as:

Angew Chem Int Ed Engl. 2022 February 21; 61(9): e202113617. doi:10.1002/anie.202113617.

A Dual-Color Fluorescent Probe Allows Simultaneous Imaging of Main and Papain-like Proteases of SARS-CoV-2-Infected Cells for Accurate Detection and Rapid Inhibitor Screening

Yong Cheng[a], **Raina M. Borum**[a], **Alex E. Clark**[c], **Zhicheng Jin**[a], **Colman Moore**[a], **Pavla Fajtová**[d], **Anthony J. O'Donoghue**[d], **Aaron F. Carlin**[c], **Jesse V. Jokerst**[a,b,e]

[a] Department of NanoEngineering, University of California, San Diego, La Jolla, CA 92093, USA

[b] Materials Science and Engineering Program, University of California, San Diego, La Jolla, CA 92093, USA

[c] Department of Medicine, University of California, San Diego, La Jolla, CA 92093, USA

[d] Skaggs School of Pharmacy and Pharmaceutical Sciences, University of California, San Diego, La Jolla, CA 92093, USA

[e] Department of Radiology, University of California, San Diego, La Jolla, CA 92093, USA

Abstract

The main protease (M^{pro}) and papain-like protease (PL^{pro}) play critical roles in SARS-CoV-2 replication and are promising targets for antiviral inhibitors. Simultaneous visualization of M^{pro} and PL^{pro} is extremely valuable for SARS-CoV-2 detection and rapid inhibitor screening. However, such a crucial investigation has remained challenging because the lack of suitable probes. Here we developed a dual-color probe named 3MBP5 for simultaneous detection of M^{pro} and PL^{pro} via fluorescence (or Förster) resonance energy transfer (FRET). This probe produces fluorescence from both of Cy3 and Cy5 fluorophores cleaved by M^{pro} and PL^{pro}. 3MBP5 activatable specificity was demonstrated with recombinant proteins, inhibitors, plasmid transfected HEK 293T cells, and SARS-CoV-2 infected TMPRSS2-Vero cells. Results from dual-color probe first verified simultaneous detection and intracellular distribution of SARS-CoV-2 M^{pro} and PL^{pro}. This is a powerful tool for simultaneous detection of different proteases with value in rapid screening of inhibitors.

Graphical Abstract

jjokerst@eng.ucsd.edu .

Conflict of interest

The authors declare no conflict of interest.

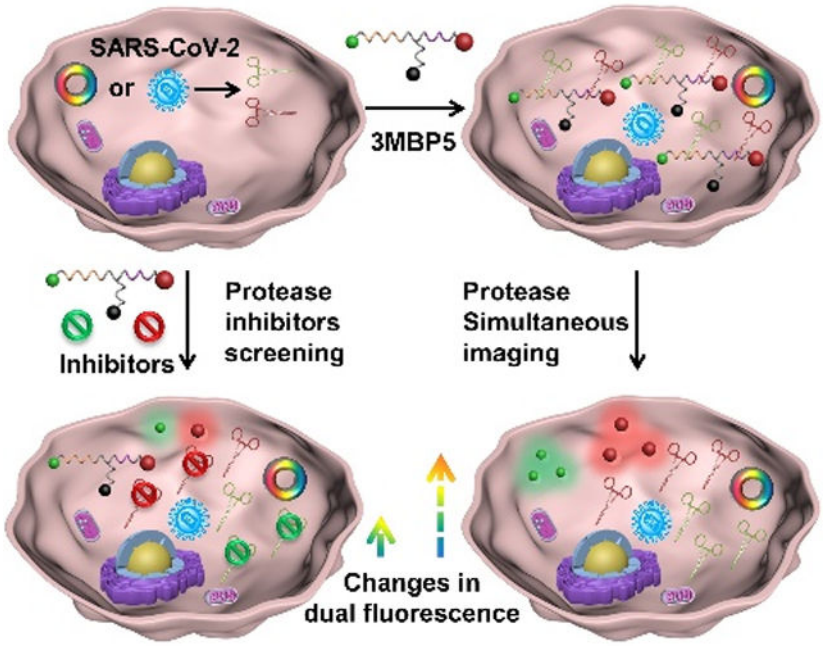

Simultaneous visualizing of crucial proteases within the SARS-CoV-2 infected cells can be significant benefit to accurate virus detection and rapid inhibitor screening as well as understanding the viral lifecycle. The catalytic efficiency, intracellular enzyme activity and distribution of SARS-CoV-2 main protease and papain-like protease are exploited with peptide-based dual-color FRET probes and their inhibitors.

Keywords

main protease; papain-like protease; SARS-CoV-2; simultaneous visualizing; inhibitor screening

Introduction

The coronavirus disease 2019 (COVID-19) pandemic caused by severe acute respiratory syndrome coronavirus 2 (SARS-CoV-2) continues to threaten global health.[1, 2] Detection of SARS-CoV-2 RNAs and antibodies have been widely explored by quantitative reverse transcription polymerase chain reaction, isothermal nucleic acid amplification methods, lateral flow assays, and electrochemical chips.[3] Understanding the viral lifecycle and distribution of relevant proteases are critical to controlling disease propagation, diagnosing infection, and screening therapies. The main protease (M^{pro}, also known as $3CL^{pro}$) and papain-like protease (PL^{pro}) are specifically encoded from the open-reading frames (ORFs) of coronavirus RNA genome.[4, 5] M^{pro} and PL^{pro} are essential non-structural proteins (NSPs) for processing the viral precursor polyprotein to form functional proteins during viral replication. Their amino acid sequences are highly conserved in SARS-CoV, SARS-CoV-2, and Middle East respiratory syndrome (MERS).[6] Importantly, these enzymes are

not closely related to any human protease making them selective biomarkers for virus detection and drug development, because targeting M^{pro} and PL^{pro} are unlikely to target the host proteases. However, the potential spatial and temporal distribution as well as their functionalities of M^{pro} and PL^{pro} in SARS-CoV-2-infected cells remains unclear.[7]

Numerous methods have been applied to simultaneously detect multiple biomarkers in complex biological samples, such as recombinant fluorescent proteins, nanoparticle-based optical and electrochemical sensors.[8] Among them, fluorescence (or Förster) resonance energy transfer (FRET) probes that report biochemical processes in living cells have generated great interest because of their rapid signal acquisition, high detection sensitivity, low background and noninvasiveness.[9] Furthermore, multicolor FRET (mFRET) has been broadly used to determine distances, structures, interactions and dynamics of multiple biomolecules.[10] M^{pro} cleaves viral polyproteins after the Leu-Gln (LQ) sequence, and PL^{pro} cleaves viral polyproteins after the Leu-Xaa-Gly-Gly (LXGG, where Xaa represents any amino acid) sequence.[11] PL^{pro} can remove the ubiquitin-like ISG15 protein modifications in addition to Lys_{48}-linked polyubiquitin with domain interaction to regulate viral spread and innate immunity.[12] Thus, M^{pro} and PL^{pro} are suitable targets for FRET-based detection.

There are a variety of commercially available and research-grade substrate screening tools available including several for M^{pro} and PL^{pro}. Recently reported substrates show high specificity and good selectivity.[13] However, these are all single channel screens and it can be difficult to confirm if the two different probes are internalized in the same cell at similar concentrations for precise cell imaging analysis.[14, 12a] It could be more accurate and effective to image both proteases with a dual-color FRET probe. However, no such probe is available for M^{pro} and PL^{pro} simultaneous detection despite potential value in understanding virus lifecycle and treatment impact due to simultaneous imaging of M^{pro} and PL^{pro} in SARS-CoV-2-infected cells.

Here we designed and synthesized a dual-color fluorescent probe named 3MBP5 for simultaneous visualization of M^{pro} and PL^{pro} in the SARS-CoV-2 infected cells. 3MBP5 involves five segments (Scheme 1a): (1) a fluorophore Cyanine3 (Cy3, **3**), (2) a M^{pro}-responsive peptide (SAVLQ/SGFRKMA, **M**), (3) a black hole quencher-2 (BHQ-2, **B**), (4) a PL^{pro}-responsive peptide (RLRGG/K, P), and (5) another fluorophore Cyanine5 (Cy5, **5**).

The bold parts are abbreviated as **3MBP5**. These components were covalently linked using a combination of Fmoc-based solid-phase peptide synthesis, thiol−maleimide Michael addition and copper-catalyzed azide-alkyne click reaction. The fluorescence of 3MBP5 at both Cy3 and Cy5 channels is effectively quenched by BHQ-2 when peptide is intact (Scheme 1b). After cleavage by M^{pro} and PL^{pro}, fluorescence intensities of Cy3 and Cy5 will significantly increase since they are no longer quenched by BHQ-2. Upon addition of M^{pro} and PL^{pro} inhibitors, protease activities of M^{pro} and PL^{pro} are inhibited, and fluorescence signals of Cy3 and Cy5 will decrease with the increasing inhibitor concentrations. Therefore, the activities of M^{pro}, PL^{pro} and their inhibitors can be monitored by fluorescence changes. This well-designed and robust dual-color probe will provide a novel avenue for simultaneous protease detection and rapid inhibitor screening.

Results and Discussion

To simultaneously detect M^{pro} and PL^{pro} in vitro and in cells, commercial fluorescent dyes Cy3, Cy5 and BHQ-2 were chosen as optimal FRET pairs according to their sizable overlaps of absorption and emission spectra.[15] Cy3 and Cy5 showed strong absorption spectral profiles at 450–580 nm and 550–700 nm in a mixed solution of DMSO/water (v/v = 1:99) at room temperature (Supporting Information Figure S1). To avoid overlap of emission spectra between Cy3 and Cy5, 500 nm for Cy3 and 600 nm for Cy5 were selected as the optimal excitation wavelengths. The fluorescence spectral profiles of Cy3 and Cy5 were from 530–700 nm and 630–800 nm. Taking spatial distance between donor and acceptor into consideration, we designed 3MBP5 with two donors (Cy3 and Cy5) at the two ends of protease-cleavable peptide; and one acceptor (BHQ-2) in the center.[16] We then chose Cy3-BHQ-2 pair for M^{pro} detection and Cy5-BHQ-2 pair for PL^{pro} detection based on FRET efficiency (E_{FRET}) and substrate length (Scheme S1). The experimental calculated Förster radii (rDA) is smaller than the estimated Förster radius (RDA) indicating FRET between Cy3-Cy5 (4.40 nm < 6.20 nm), Cy3-BHQ-2 (2.73 nm < 5.09 nm), and Cy5-BHQ-2 (3.48 nm < 4.75 nm) (Table S1).[17] Furthermore, the lowest energy structure and center-to-center separation distance were analyzed by Molecular Operating Environment (MOE) software (Figure S2). The extracted donor-acceptor distances agreed well with the molecular simulations, and indicated that Cy3, Cy5 and BHQ-2 can be recruited for dual-color FERT probe.

Azide-functionalized BHQ-2 was first synthesized (Scheme S2). Cysteine (Cys) and propargylglycine (Pra) linkers were reacted with maleimide- and azide-functionalized dyes, respectively. Glycine (Gly) spacers were used to enhance molecular flexibility and reduce steric hindrance (Scheme S3). [18] Before cleavage off the resin, Cy3 was linked to Gly on the N-terminus via an amidation. Then, maleimide-functionalized Cy5 was coupled to Cys via a thiol−maleimide Michael addition. Finally, azide-functionalized BHQ-2 was covalently bound to Pra via a copper-catalyzed azide-alkyne click reaction.[19]

Control probes verified substrate specificity and enzyme activity with Cy5-BHQ-2 pair: BRM5 (**R** stands for the abbreviation of tetra-polyarginine) for M^{pro} detection, BRP5 for PL^{pro} detection, and 3EBP5. Here, **E** is the abbreviation of the M^{pro}-responsive sequence with a Gln to Glu mutation to prevent the M^{pro}-substrate interactions) for PL^{pro} detection (Figure 1a, Scheme S4, S5, S6). A hydrophilic tetra-polyarginine was incorporated into BRM5 and BRP5 in order to enhance their solubility and cell permeability.[20] This motif can promote probe entry into cells and reduce probe degradation in the cell microenvironment.

All products were purified by high performance liquid chromatography (HPLC) (Figure 1b). Their chemical structures were characterized by electrospray ionization mass spectrometry (ESI-MS) or nuclear magnetic resonance spectroscopy (NMR) (Figure 1c, S3–S9). Taking 3MBP5 as an example as shown in Figure 1c, a strong peak at 832.2641 attributed to $[M+5H]^{5+}$ of 3MBP5 (calculated, 832.0489), a strong peak at 693.7515 attributed to $[M+6H]^{6+}$ ion of 3MBP5 (calculated, 693.5421), and a strong peak at 594.7490 attributed to $[M+7H]^{7+}$ ion of 3MBP5 (calculated, 594.6086). Importantly, exact molecular weights of

a hydrolysis of five-membered rings from maleimide-functionalized Cy5 can be observed in mass spectra of 3EP5, 3MP5, 3EBP5, and 3MBP5 due to the reversible thiol-maleimide conjugation reaction (Figure S10, S11).[21] These results confirmed that 3MBP5, 3EBP5, BRM5, and BRP5 were successfully synthesized.

We evaluated whether these probes can be specifically cleaved by recombinant M^{pro} and PL^{pro}. HPLC and ESI-MS results showed that BRM5 and 3MBP5 probes were cleaved by M^{pro} after the AVLQ site with incubation for 1 h at 37 °C in 20 mM Tri-HCl buffer (pH 8.0). The cleavage efficiency of BRM5 and 3MBP5 by M^{pro} was 85.52% and 93.39%, respectively (Figure S12–S14, S18). Under the same assay conditions, BRP5 and 3MBP5 probes were cleaved by PL^{pro} after the RLRGG site, but the cleavage efficiency was 54.34% and 12.63%, respectively (Figure S15–S17, S19–S22). These results demonstrated that 3MBP5 can be cleaved by both M^{pro} and PL^{pro} at engineered sites with different efficiencies, and PLpro activity was greatly affected by chemical structure.

We then studied the potential optical spectral properties of 3MBP5 with M^{pro}, PL^{pro} and their inhibitors (Figure 2a). BHQ-2 showed wide range of absorption spectral profiles at 400–720 nm (Figure 2b). The fluorescence intensity of Cy5 but not Cy3 in 3MP5 obviously enhanced with 500 nm excitation, revealing significant FRET effect between Cy3 and Cy5 (yellow line, Figure 2c). After being modified with BHQ-2, fluorescence intensities of Cy3 and Cy5 in 3MBP5 obviously decreased due to effective quenching efficiency of BHQ-2 (pink lines, Figure 2c, 2d). According to fluorescence changes of Cy5 before and after modification with peptide and BHQ-2 in BRM5, suggesting 2 μM of probe was optimal concentration for protease detection (Figure S23). In addition, BRM5, BRP5, 3EBP5, and 3MBP5 were incubated with different concentrations of M^{pro} and PL^{pro} to validate probe sensitivity. As seen in Figure 2e, 2f, S24, and S25, fluorescence intensities of BRM5 and 3MBP5 but not 3EBP5 were gradually enhanced with increasing M^{pro} concentration. BRP5, 3EBP5, and 3MBP5 were all activated by PL^{pro}.

Kinetic studies of 3MBP5 incubation with M^{pro} and PL^{pro} were recorded over time. The fluorescence intensity at 560 nm (500 nm excitation) of 3MBP5 peaked within 20 min for M^{pro} incubation (Figure 2g), but it took more than 3 h to achieve maximum fluorescence at 660 nm (600 nm excitation) for PL^{pro} incubation (Figure 2h). We evaluated three different sources of PL^{pro} protease and noted similar results (Figure S26, S27). Next, 3MBP5, BRM5 and BRP5 were treated with different control proteins under identical conditions to investigate selectivity: thrombin (TB), hemoglobin (HGB), and bovine serum albumin (BSA) (Figure 2i, 2j, S28). Cy3 and Cy5 fluorescence intensities in 3MBP5 were obviously enhanced only when incubated with M^{pro} and PL^{pro}. In the Cy3 channel, M^{pro} and PL^{pro} co-incubation for both BRM5 and 3MBP5 led to much stronger fluorescence intensity than M^{pro} incubation alone resulting in 33.6% and 40.4% fluorescence enhancement. In the Cy5 channel, however, the fluorescence intensity showed negligible change after BRP5, 3EBP5, and 3MBP5 were co-incubated with M^{pro} and PL^{pro} compared to PL^{pro} incubation alone. The obvious color changes were observed after 3MBP5 was incubated with different concentration of M^{pro} for 1 h at room temperature (25 °C, Figure S29). Thin layer chromatography (TLC) tests showed more probe cleavage when 3MBP5 was co-incubated with M^{pro} and PL^{pro} than M^{pro} incubation alone. These results confirmed that 3MBP5 can

quantitatively detect both M^{pro} and PL^{pro} together, and PL^{pro} can promote M^{pro} cleavage efficiency when co-incubation.

Commercial inhibitors GC376 for M^{pro} and GRL0617 for PL^{pro} were used to confirm whether the probes can be used for M^{pro} and PL^{pro} inhibitor screening.[5, 13b, 12] Different concentrations of inhibitors were incubated with a fixed concentration of M^{pro} (100 nM) and PL^{pro} (1.0 μM) and 2.0 μM BRM5, 2.0 μM BRP5, and 2.0 μM 3MBP5 for 1 h at 37 °C in 20 mM Tri-HCl buffer (pH 8.0). The fluorescence changes were recorded (Figure 2k, 2l and S30); both Cy3 and Cy5 signals significantly reduced with increasing inhibitor concentrations. The results demonstrated that 3MBP5 can simultaneously detect M^{pro} and PL^{pro} inhibitors and thus hold potential for rapid inhibitor screening.

We next used 3MBP5 for cell imaging. HEK 293T cells were transfected with three different plasmids: A SARS-CoV-2 M^{pro} plasmid, a SARS-CoV-2 PL^{pro} plasmid, and a control influenza virus protein (A/PR8/1834 NP, referred to PR8) plasmid.[13b] The plasmid transfected HEK 293T cells were subsequently incubated with different probes, and M^{pro} and PL^{pro} inhibitors for confocal laser scanning microscopy (CLSM) observation (Figure 3a). The cell imaging incubation time, probe concentration, and optical parameters of Cy3 and Cy5 were optimized first. Different concentrations (1.0 μM, 2.0 μM, 4.0 μM, and 8.0 μM) of Cy3 and Cy5 were co-incubated with HEK 293T cells for 3 h under standard cell culture conditions (Figure S31). The commercial dye Hoechst 33258 was chosen to stain the nuclei of cells. According to CLSM images and cytotoxicity analysis, 2.0 μM Cy5 was sufficient and suitable for cell imaging. Higher concentrations of Cy5 may result in high background and cytotoxicity (Figure S32). Additionally, to validate non-specific cleavage and avoid false positive signals, 2.0 μM 3MBP5 was incubated with Dulbecco's modified eagle medium (DMEM) (Figure. S33). DMEM alone does not activate the probe. Cy3 but not Cy5 fluorescence signal of 3MBP5 rapidly increased within 15 min in DMEM with M^{pro}. 10% FBS in DMEM cleaves the peptide after 30 min incubation, and its maximum fluorescence was reached after 95 min incubation. This cleavage is significantly slower (80 min) than that detected for M^{pro}. The results indicate that (i) M^{pro} is more robust and active than PL^{pro} in cell culture media and (ii) prolonged incubation times will lead to non-specific activation of 3MBP5 in complex cell culture medium. Therefore, 2.0 μM of each probe incubated for 30 min is optimal for cell imaging experiments.

To assess M^{pro} and PL^{pro} activity in plasmid transfected HEK 293T cells, CLSM cell imaging experiments were performed after incubation with 2.0 μM BRM5 and 2.0 μM BRP5 for 30 min (Figure S34 and S35). The red fluorescence of BRM5 and BRP5 were observed in M^{pro} or PL^{pro} plasmid transfected cells but not in PR8 plasmid-transfected cells. Their fluorescence intensities clearly increased with increasing plasmid concentrations. Furthermore, M^{pro} and PL^{pro} plasmid transfected cells were incubated with 2.0 μM 3MBP5 for 30 min. Compared with weak fluorescence in naked cells or PR8-transfected cells (Figure 3b and 3f), M^{pro} plasmid-transfected cells showed obvious green fluorescence (Figure 3c), and PL^{pro} plasmid transfected cells showed strong red fluorescence (Figure 3d). Only M^{pro} and PL^{pro} plasmid co-transfected cells show both green and red fluorescence leading to yellow overlap (Figure. 3e). Moreover, red fluorescence intensity enhanced with increasing ratio of plasmids between M^{pro} and PL^{pro} (Figure S36). To validate use of

3MBP5 for cell-based inhibitor screening, 10 μM M^{pro} inhibitor (GC376) and 10 μM PL^{pro} inhibitor (GRL0617) was added to the plasmid-transfected cells (Figure 3g, 3h and 3i). The green and red fluorescence decreased corresponding to inhibition of each viral protease. These data demonstrated that 3MBP5 can be used for imaging intracellular activity of M^{pro} and PL^{pro} in plasmid transfected cells and identifying protease inhibition.

After confirming that 3MBP5 could detect M^{pro} and PL^{pro} in plasmid transfected HEK 293T cells, we next determined if 3MBP5 could be used for imaging of M^{pro} and PL^{pro} and screening their inhibitors in SARS-CoV-2 infected cells. Thus, TMPRSS2-Vero cells were infected with SARS-CoV-2 (USA-WA1/2020) at a multiplicity of infection (MOI) of 0.02 for 24 h before adding the probes (Figure. 4a).[13b] At 24 h post-infection, 3MBP5 and Hoechst 33258 were added into the cells for another 30 min incubation. Versus fluorescence of noninfected cells and infected cells, strong green and red fluorescence were observed in infected cells but not in noninfected cells when incubated with 2.0 μM 3MBP5 (Figure S37). The 1.0 μM 3MBP5 could not produce fluorescence in infected cells, but 4.0 μM 3MBP5 led to strong nonspecific green and red fluorescence in uninfected cells. Therefore, 2.0 μM 3MBP5 was chosen for subsequent cell imaging.

SARS-CoV-2 infection of cells was confirmed by staining with anti-SARS-CoV-2 nucleocapsid (Capsid) and anti-SARS-CoV-2 M^{pro} primary antibodies and AlexaFluor 488-labeled secondary antibody (Alexa488). There was obvious green (M^{pro}), red (PL^{pro}), and cyan (Capsid) fluorescence in the infected cells but not in uninfected cells (Figure 4b, 4c, Videos S1 and S2). These data confirmed that the virus was present and producing proteases of interest. Interestingly, some infected cells with most Alexa488-labeled Capsid staining had little M^{pro} and PL^{pro} signal, and not all infected cells had the same degree of signal for each protease. This staining indicated that there were differences in intracellular protein expression levels between M^{pro}, PL^{pro} and Capsid.

When the infected cells were incubated with M^{pro} primary antibody, Alexa488 and 3MBP5, the green (M^{pro}), red (PL^{pro}) and cyan (M^{pro}) fluorescence had good overlap, and their fluorescence intensities varied between cells (Figure 4d and Video S3). In addition, Pearson's correlation coefficients of co-localization between green (M^{pro}), red (PL^{pro}), and cyan (capsid or M^{pro}) fluorescence increased after infection with SARS-CoV-2 (Figure S38). We can also observe some cyan fluorescence without overlap of green and red fluorescence near cell membrane (Figure 4d, pink arrow). This difference caused because 3MBP5 represented the protease activity, and Alexa488-labeled M^{pro} antibody showed the protease location. Moreover, the expression of PL^{pro}, M^{pro}, capsid, and GAPDH were confirmed by Western blot 24 h post-infection (Figure. 4i). To further evaluate the detection of protease inhibitors by 3MBP5, infected cells were incubated with different concentrations of M^{pro} inhibitor and PL^{pro} inhibitor before adding the 3MBP5. The green and red fluorescence of 3MBP5 decreased in infected cells after incubation with GC376 (Figure 4f), and the red fluorescence of 3MBP5 decreased upon incubation with GRL0617 (Figure 4g) demonstrating that a reduction in protease activity by M^{pro} inhibitor and PL^{pro} inhibitor can be detected by 3MBP5 (4f, 4g, 4h, and S39). These results confirmed that 3MBP5 could be used for simultaneous screening of both M^{pro}, PL^{pro} and their inhibitors in SARS-CoV-2 infected cells.

Conclusion

In conclusion, we report the simultaneous visualization of SARS-CoV-2 M^{pro} and PL^{pro} activity in vitro and in cells with a dual-color FRET probe. The theoretical calculations of FRET efficiencies between Cy3-BHQ-2, Cy3-Cy5, and Cy5-BHQ-2 were simulated and found to agree well with experimental results. We then successfully synthesized four different probes named 3MBP5, 3EBP5, BRM5, and BRP5—fluorogenic substrates for these proteases through Fmoc-based solid-phase peptide synthesis and click reactions. It should be possible in theory to apply this approach to respectively link three different cargoes in the same peptide and selectively deliver them into targeted sites. The LC-MS and optical property results all confirmed that the substrates could be specifically cleaved by M^{pro} and PL^{pro}. Importantly, their catalytic efficiency was first verified together with 3MBP5. This probe design could also be applied to simultaneously detect different proteases with significant value in rapid screening of inhibitors to other emerging disease by changing only the peptide cleavage sites. We also found that the intracellular distribution and content of SARS-CoV-2 nucleocapsid, M^{pro}, and PL^{pro} were different between cells. As a research tool, 3MBP5 may allow rapid identification of infected cells for sorting or verification of infection without the need to modify the virus or the host cell as with reporter genes. This method would inform future studies to accurately understand the complex biological process involving multiple proteases.

Supplementary Material

Refer to Web version on PubMed Central for supplementary material.

Acknowledgements

We thank Dr. Nicholas S. Heaton for SARS-CoV-2 M^{pro} plasmid and influenza virus protein (A/PR8/1834 NP) plasmid, Dr. Shaun K. Olsen and Dr. Tony T. Huang for SARS-CoV-2 PL^{pro}, and Dr Liangfang Zhang for HEK 293T cells. The authors thank internal funding from the UC Office of the President (R00RG2515) and the National Institutes of Health (R01 DE031114, R21 AI157957, and R21 AG065776–01S1) for financial support. This work was supported in part by the National Science Foundation Graduate Research Fellowship Program under Grant No. DGE-1650112. C.M. acknowledges support from the Achievement Reward for College Scientists (ARCS) Foundation. R.M.B. acknowledges support from the National Cancer Institute of the National Institutes of Health under the award number T32CA153915. This research was supported by NIH grant (K08 AI130381) and Career Award for Medical Scientists from the Burroughs Welcome Fund to AFC. The confocal imaging work was performed at the school of medicine microscopy and histology core of University of California San Diego, a member of the National Institute of Neurological Disorders and Stroke (NINDS), which is supported by the National Science Foundation (Grant NS047101). The following reagent was deposited by the Centers for Disease Control and Prevention and obtained through BEI Resources, NIAID, NIH: SARS-Related Coronavirus 2, Isolate USA-WA1/2020, NR-52281.

References

[1]. Lu R, Zhao X, Li J, Niu P, Yang B, Wu H, Wang W, Song H, Huang B, Zhu N, Bi Y, Ma X, Zhan F, Wang L, Hu T, Zhou H, Hu Z, Zhou W, Zhao L, Chen J, Meng Y, Wang J, Lin Y, Yuan J, Xie Z, Ma J, Liu WJ, Wang D, Xu W, Holmes EC, Gao GF, Wu G, Chen W, Shi W, Tan W, The Lancet. 2020, 395, 565–574.

[2]. Wu F, Zhao S, Yu B, Chen YM, Wang W, Song ZG, Hu Y, Tao ZW, Tian JH, Pei YY, Yuan ML, Zhang YL, Dai FH, Liu Y, Wang QM, Zheng JJ, Xu L, Holmes EC, Zhang YZ, Nature. 2020, 579, 265–269. [PubMed: 32015508]

[3]. (a)Xiong E, Jiang L, Tian T, Hu M, Yue H, Huang M, Lin W, Jiang Y, Zhu D, Zhou X, Angew. Chem. Int. Ed. Engl. 2021, 60, 5307–5315; [PubMed: 33295064] (b)Yousefi H, Mahmud A, Chang D, Das J, Gomis S, Chen JB, Wang H, Been T, Yip L, Coomes E, Li Z, Mubareka S, McGeer A, Christie N, Gray-Owen S, Cochrane A, Rini JM, Sargent EH, Kelley SO, J. Am. Chem. Soc. 2021, 143, 1722–1727; [PubMed: 33481575] (c)Kevadiya BD, Machhi J, Herskovitz J, Oleynikov MD, Blomberg WR, Bajwa N, Soni D, Das S, Hasan M, Patel M, Senan AM, Gorantla S, McMillan J, Edagwa B, Eisenberg R, Gurumurthy CB, Reid SPM, Punyadeera C, Chang L, Gendelman HE, Nat. Mater. 2021, 20, 593–605; [PubMed: 33589798] (d)Talebian S, Wallace GG, Schroeder A, Stellacci F, Conde J, Nat. Nanotechnol. 2020, 15, 618–621; [PubMed: 32728083] (e)Liu T, Hsiung J, Zhao S, Kost J, Sreedhar D, Hanson CV, Olson K, Keare D, Chang ST, Bliden KP, Gurbel PA, Tantry US, Roche J, Press C, Boggs J, Rodriguez-Soto JP, Montoya JG, Tang M, Dai H, Nat. Biomed. Eng. 2020, 4, 1188–1196. [PubMed: 33122853]

[4]. (a)Jin Z, Du X, Xu Y, Deng Y, Liu M, Zhao Y, Zhang B, Li X, Zhang L, Peng C, Duan Y, Yu J, Wang L, Yang K, Liu F, Jiang R, Yang X, You T, Liu X, Yang X, Bai F, Liu H, Liu X, Guddat LW, Xu W, Xiao G, Qin C, Shi Z, Jiang H, Rao Z, Yang H, Nature. 2020, 582, 289–293; [PubMed: 32272481] (b)Muramatsu T, Takemoto C, Kim YT, Wang H, Nishii W, Terada T, Shirouzu M, Yokoyama S, Proc. Natl. Acad. Sci. U S A. 2016, 113, 12997. [PubMed: 27799534] (c)Anand K, Ziebuhr J, Wadhwani P, Mesters JR, Hilgenfeld R, Science. 2003, 300, 1763–1767. [PubMed: 12746549]

[5]. Rut W, Lv Z, Zmudzinski M, Patchett S, Nayak D, Snipas SJ, El Oualid F, Huang TT, Bekes M, Drag M, Olsen SK, Sci. Adv. 2020, 6, eabd4596. [PubMed: 33067239]

[6]. (a)Domling A, Gao L, Chem. 2020, 6, 1283–1295; [PubMed: 32529116] (b)Pillaiyar T, Manickam M, Namasivayam V, Hayashi Y, Jung SH, J. Med. Chem. 2016, 59, 6595–6628; [PubMed: 26878082] (c)Baez-Santos YM, St John SE, Mesecar AD, Antiviral. Res. 2015, 115, 21–38. [PubMed: 25554382]

[7]. (a)Yan S, Wu G, FASEB. J. 2021, 35, e21197; [PubMed: 33368679] (b)Zohar T, Loos C, Fischinger S, Atyeo C, Wang C, Slein MD, Burke J, Yu J, Feldman J, Hauser BM, Caradonna T, Schmidt AG, Cai Y, Streeck H, Ryan ET, Barouch DH, Charles RC, Lauffenburger DA, Alter G, Cell. 2020, 183, 1508–1519. [PubMed: 33207184]

[8]. (a)Frei AP, Bava FA, Zunder ER, Hsieh EW, Chen SY, Nolan GP, Gherardini PF, Nat. Methods. 2016, 13, 269–275; [PubMed: 26808670] (b)Canales A, Jia X, Froriep UP, Koppes RA, Tringides CM, Selvidge J, Lu C, Hou C, Wei L, Fink Y, Anikeeva P, Nat. Biotechnol. 2015, 33, 277–284; [PubMed: 25599177] (c)Zhou L, Wang R, Yao C, Li X, Wang C, Zhang X, Xu C, Zeng A, Zhao D, Zhang F, Nat. Commun. 2015, 6, 6938 [PubMed: 25907226] (d)Lam AJ, St-Pierre F, Gong Y, Marshall JD, Cranfill PJ, Baird MA, McKeown MR, Wiedenmann J, Davidson MW, Schnitzer MJ, Tsien RY, Lin MZ, Nat. Methods. 2012, 9, 1005–1012; [PubMed: 22961245] (e)Mi LZ, Lu C, Li Z, Nishida N, Walz T, Springer TA, Nat. Struct. Mol. Biol. 2011, 18, 984–989; [PubMed: 21822280] (f)Andresen M, Stiel AC, Fölling J, Wenzel D, Schönle A, Egner A, Eggeling C, Hell SW, Jakobs S, Nat. Biotechnol. 2008, 26, 1035–1040. [PubMed: 18724362]

[9]. (a)Li J, Pu K, Chem. Soc. Rev. 2019, 48, 38–71; [PubMed: 30387803] (b)Ye D, Shuhendler AJ, Cui L, Tong L, Tee SS, Tikhomirrov G, Felsher DW, Rao J, Nat. Chem. 2014, 6, 519–526; [PubMed: 24848238] (c)Pu K, Shuhendler AJ, Rao J, Angew. Chem. Int. Ed. Engl. 2013, 52, 10325–10329; [PubMed: 23943508] (d)Razgulin A, Ma N, Rao J, Chem. Soc. Rev. 2011, 9, 4186–4216;(e)Lovell JF, Liu TWB, Chen J, Zheng G, Chem. Rev. 2010, 110, 2839–2857. [PubMed: 20104890]

[10]. (a)Widen JC, Tholen M, Yim JJ, Antaris A, Casey KM, Rogalla S, Klaassen A, Sorger J, Bogyo M, Nat. Biomed. Eng. 2021, 5, 264–277; [PubMed: 32989286] (b)Dagher M, Kleinman M, Ng A, Juncker D, Nat. Nanotechnol. 2018, 13, 925–932; [PubMed: 30061659] (c)Ma Y, Yamamoto Y, Nicovich PR, Goyette J, Rossy J, Gooding JJ, Gaus K, Nat. Biotechnol. 2017, 35, 363–370. [PubMed: 28288102]

[11]. (a)El-Baba TJ, Lutomski CA, Kantsadi AL, Malla TR, John T, Mikhailov V, Bolla JR, Schofield CJ, Zitzmann N, Vakonakis I, Robinson CV, Angew. Chem. Int. Ed. Engl. 2020, 59, 23544–23548; [PubMed: 32841477] (b)Ma-Lauer Y, Carbajo-Lozoya J, Hein MY, Muller MA, Deng W, Lei J, Meyer B, Kusov Y, von Brunn B, Bairad DR, Hunten S, Drosten C, Hermeking H, Leonhardt H, Mann M, Hilgenfeld R, von Brunn A, Proc. Natl. Acad. Sci. U S A. 2016, 113,

E5192–E5201; [PubMed: 27519799] (c)Bekes M, van der Heden van Noort GJ, Ekkebus R, Ovaa H, Huang TT, Lima CD, Mol. Cell. 2016, 62, 572–585. [PubMed: 27203180]

[12]. (a)Shin D, Mukherjee R, Grewe D, Bojkova D, Baek K, Bhattacharya A, Schulz L, Widera M, Mehdipour AR, Tascher G, Geurink PP, Wilhelm A, van der Heden van Noort GJ, Ovaa H, Muller S, Knobeloch KP, Rajalingam K, Schulman BA, Cinatl J, Hummer G, Ciesek S, Dikic I, Nature. 2020, 587, 657–662; [PubMed: 32726803] (b)Ratia K, Pegan S, Takayama J, Sleeman K, Coughlin M, Baliji S, Chaudhuri R, Fu W, Prabhakar BS, Johnson ME, Baker SC, Ghosh AK, Mesecar AD, Proc. Natl. Acad. Sci. USA. 2008, 105, 16119–16124. [PubMed: 18852458]

[13]. (a)Rut W, Groborz K, Zhang L, Sun X, Zmudzinski M, Pawlik B, Wang X, Jochmans D, Neyts J, Mlynarski W, Hilgenfeld R, Drag M, Nat. Chem. Biol. 2021, 17, 222–228; [PubMed: 33093684] (b)Froggatt HM, Heaton BE, Heaton NS, J. Virol. 2020, 94, e01265–20; [PubMed: 32843534] (c)Wang L, Hu W, Fan C, Protein. Sci. 2020, 29, 1228–1241. [PubMed: 32216114]

[14]. (a)Penalver L, Schmid P, Szamosvari D, Schildknecht S, Globisch C, Sawade K, Peter C, Bottcher T, Angew. Chem. Int. Ed. Engl. 2021, 60, 6799–6806; [PubMed: 33350010] (b)Steuten K, Kim H, Widen JC, Babin BM, Onguka O, Lovell S, Bolgi O, Cerikan B, Neufeldt CJ, Cortese M, Muir RK, Bennett JM, Geiss-Friedlander R, Peters C, Bartenschlager R, Bogyo M, ACS. Infect. Dis. 2021, 7, 1457–1468. [PubMed: 33570381]

[15]. (a)Cho Y, An HJ, Kim T, Lee C, Lee NK, J. Am. Chem. Soc. 2021, 143, 14125; [PubMed: 34432445] (b)Sun W, Guo S, Hu C, Fan J, Peng X, Chem. Rev. 2016, 116, 7768–7817; [PubMed: 27314280] (c)Lu CH, Cecconello A, Elbaz J, Credi A, Willner I, Nano. Lett. 2013, 13, 2303–2308. [PubMed: 23557381]

[16]. (a)Zhang C, Dong X, Ong SY, Yao SQ, Anal. Chem. 2021, 93, 12081–12089; [PubMed: 34436865] (b)Xue L, Prifti E, Johnsson K, J. Am. Chem. Soc. 2016, 138, 5258–5261; [PubMed: 27071001] (c)Jia X, Chen Q, Yang Y, Tang Y, Wang R, Xu Y, Zhu W, Qian X, J. Am. Chem. Soc. 2016, 138, 10778–10781. [PubMed: 27517310]

[17]. Clapp AR, Medintz IL, Mauro JM, Fisher BR, Bawendi MG, Mattoussi H, J. Am. Chem. Soc. 2004, 126, 301–310. [PubMed: 14709096]

[18]. (a)Chen X, Zaro JL, Shen WC, Adv. Drug. Deliv. Rev. 2013, 65, 1357–1369; [PubMed: 23026637] (b)Reddy Chichili VP, Kumar V, Sivaraman J, Protein. Sci. 2013, 22, 153–167. [PubMed: 23225024]

[19]. (a)Cheng Y, Sun C, Liu R, Yang J, Dai J, Zhai T, Lou X, Xia F, Angew. Chem. Int. Ed. Engl. 2019, 58, 5049–5053; [PubMed: 30767348] (b)Cheng Y, Sun C, Ou X, Liu B, Lou X, Xia F, Chem. Sci. 2017, 8, 4571–4578; [PubMed: 28626568] (c)Cheng Y, Huang F, Min X, Gao P, Zhang T, Li X, Liu B, Hong Y, Lou X, Xia F, Anal. Chem. 2016, 88, 8913–8919. [PubMed: 27503607]

[20]. (a)Zhang P, Cui Y, Anderson CF, Zhang C, Li Y, Wang R, Cui H, Chem. Soc. Rev. 2018, 47, 3490–3529; [PubMed: 29497722] (b)Peraro L, Kritzer JA, Angew. Chem. Int. Ed. Engl. 2018, 57, 11868–11881; [PubMed: 29740917] (c)Stewart MP, Sharei A, Ding X, Sahay G, Langer R, Jensen KF, Nature. 2016, 538, 183–192. [PubMed: 27734871]

[21]. Lyon RP, Setter JR, Bovee TD, Doronina SO, Hunter JH, Anderson ME, Balasubramanian CL, Duniho SM, Leiske CI, Li F, Senter PD, Nat. Biotechnol. 2014, 32, 1059–1062. [PubMed: 25194818]

a

Name	Sequence	Protease
3MBP5	(Cy3)GSAVLQ/SGFRKMAG(Pra)(BHQ-2)GRLRGG/KGC(Cy5)	M^{pro}/PL^{pro}
3EBP5	(Cy3)GSAVLESGFRKMAG(Pra)(BHQ-2)GRLRGG/KGC(Cy5)	PL^{pro}
BRP5	(BHQ-2)GRRRRGRLRGG/KG(Pra)(Cy5)	PL^{pro}
BRM5	(BHQ-2)RRRRSAVLQ/SGFRKMA(Pra)(Cy5)	M^{pro}

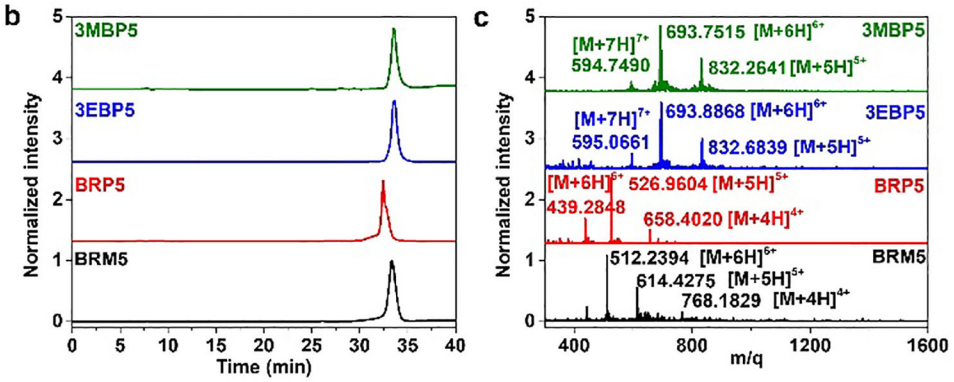

Figure 1. Characteristics of 3MBP5 and its derivatives.

(a) Molecular structures and peptide sequences, (b) high-performance liquid chromatography (HPLC), and (c) electrospray ionization mass spectra (ESI-MS) results of 3MBP5, 3EBP5, BRP5, and BRM5 confirm that all probes were prepared with at least 95% purity. The orange peptide sequence represents M^{pro} binding and cleavage fraction. The pink peptide sequence represents PL^{pro} binding and cleavage fraction. The slash represents the protease cleavage site.

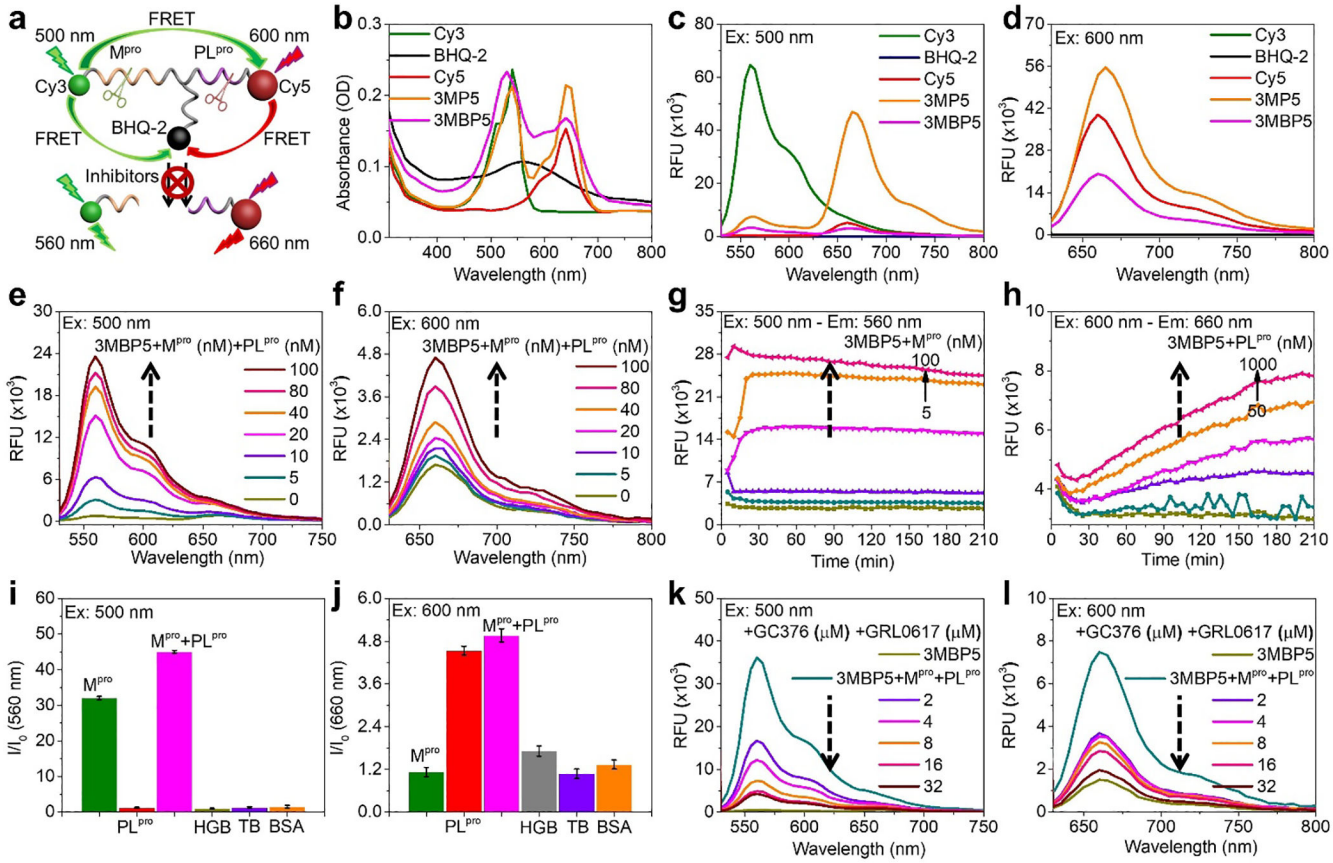

Figure 2. Photophysical properties and probe activation via proteases.

(a) Schematic representation of FRET effect between Cy3, Cy5, and BHQ-2 in 3MBP5 with M^{pro}, PL^{pro}, and inhibitors. (b-d) UV−vis absorption and fluorescence spectra of 10 μM of Cy3, BHQ-2, Cy5, 3MP5, and 3MBP5 showed good spectral overlap for FRET. (e-f) Fluorescence spectra and (g-h) fluorescent kinetics of 2.0 μM 3MBP5 with M^{pro} and PL^{pro} showed dual-color fluorescence signal increase. (i-j) Probe specificity to the target M^{pro} and PL^{pro} as shown via fluorescence response of 2.0 μM 3MBP5 with 100 nM of M^{pro}, PL^{pro}, M^{pro} and PL^{pro}, thrombin (TB), hemoglobin (HGB), and bovine serum albumin (BSA). (k-l) Impact of protease inhibitors as studied via 2.0 μM 3MBP5 with 100 nM M^{pro}, 1.0 μM PL^{pro}, GC376, and GRL0617; the inhibitor decreased the 3MBP5 signal. In k and l, the turquoise line is no inhibitor, and the taupe line is probe only (no protease, no inhibitor). All other colors represent different inhibitor concentrations. For all panels, the probes were dissolved in Tris-HCl buffer with 1% DMSO. The excitation wavelength for Cy3 is 500 nm in Figure c, e, g, i and k. The excitation wavelength for Cy5 is 600 nm in Figure d, f, h, j and l.

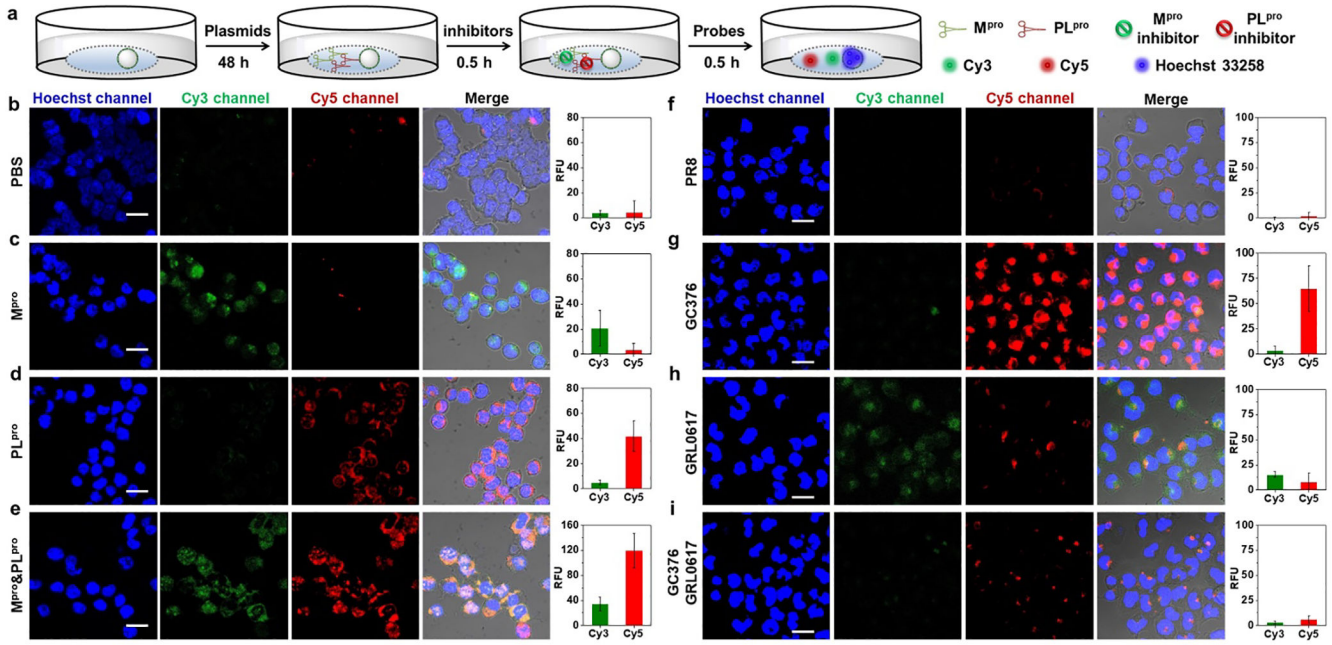

Figure 3. Validation of 3MBP5 via plasmids and inhibitors.

Confocal laser scanning microscopy (CLSM) images and mean fluorescence intensity of HEK 293T cells incubated with PR8, M^{pro}, and PL^{pro} plasmids as well as the impact of inhibitors. (a) Experimental scheme of HEK 293T cells incubated with plasmids, inhibitors, and probes in DMEM without FBS. (b) 3MBP5 and PBS show that there is no background activation of 3MBP5. (c) 3MBP5 is activated in the green channel when the cells are cultured with the M^{pro} plasmid. (d) 3MBP5 is activated in the red channel when cells are incubated with PL^{pro} plasmid. (e) 3MBP5 produces signal in both red and green channels when cells are incubated with both M^{pro} and PL^{pro} plasmids. (f) 3MBP5 was added to cells treated with a control plasmid (PR8)—the results show no signal activation. (g) The GC376 M^{pro} inhibitor decreased activity of M^{pro} and led to a decrease in green emission of 3MBP5. (h) The GRL0617 PL^{pro} inhibitor decreased activity of PL^{pro} and led to a decrease in red emission of 3MBP5. (i) The use of both inhibitors caused both signal channels to decrease. All scale bars are 20 μm.

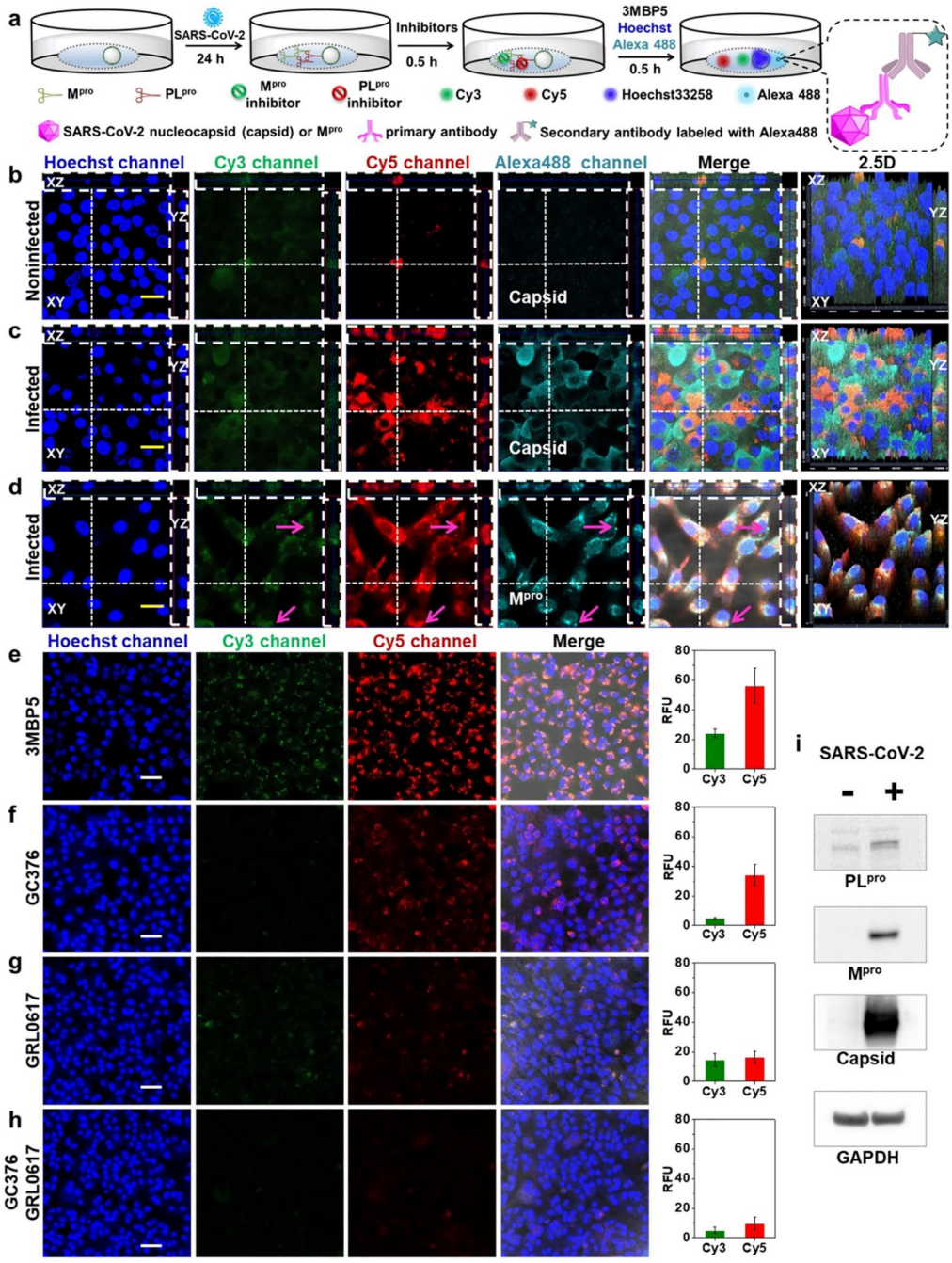

Figure 4. Simultaneous visualization of M^{pro}, PL^{pro}, and inhibitors in SARS-CoV-2-infected TMPRSS2-Vero cells.

(a) Experimental scheme of SARS-CoV-2-infected cells were incubated with different probes and inhibitors. Enlarged view shows the imaging mechanism with Alexa488 (b) Noninfected cells and (c) infected cells were incubated with 3MBP5, anti-SARS-CoV-2 nucleocapsid (Capsid) primary antibody, and Alexa488 labeled secondary antibody. Panel b shows no false positive signal activation. Panel c confirms that the 3MBP5 can image M^{pro} and PL^{pro} from actual SARS-CoV-2 viruses and that the virus is present (via capsid immunostaining). In panel d, the immunostaining is for M^{pro} protein as an independent

confirmation that the target is present. Panels e-h show the Impact of inhibitors in SARS-CoV-2-infected cells: (e) no inhibitors, (f) GC376 M^{pro} inhibitor, (g) GRL0617 PL^{pro} inhibitor, and (h) both inhibitors. The results confirm that signal decreases when target increases. (i) Western blotting of M^{pro}, PL^{pro}, Capsid, and GAPDH in noninfected and infected cells after 24 h of infection again confirming the presence/absence of target. All the nuclei were stained with 5 μM Hoechst33258. The yellow scale bar is 20 μm. The white scale bar is 50 μm. The vertical dotted line means YZ plane cutting line. The transverse dotted line means XZ plane cutting line. The pink arrow shows obvious fluorescence only from Alexa488.

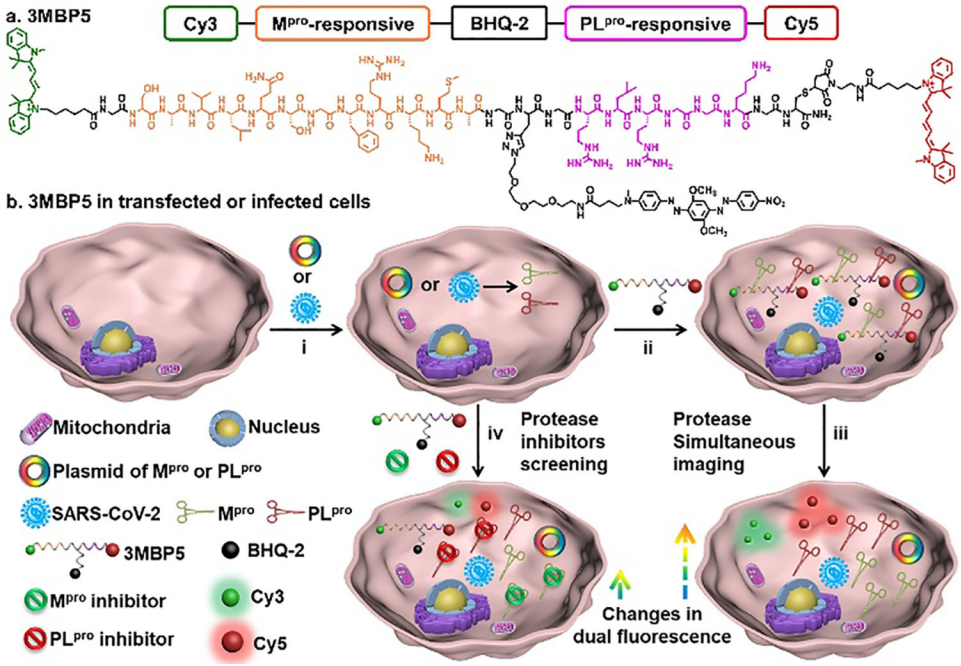

Scheme 1. Structure and function of 3MBP5.

(a) Molecular structure of 3MBP5. (b) 3MBP5 is used for simultaneous visualization of SARS-CoV-2 M^{pro} and PL^{pro}, and rapid inhibitor screening. i) M^{pro} and PL^{pro} plasmids transfected or SARS-CoV-2-infected cells can produce M^{pro} and PL^{pro}; ii) 3MBP5 were incubated with the transfected or infected cells; iii) After being cleaved by M^{pro} and PL^{pro}, fluorescence of Cy3 and Cy5 fragments recovered without spatial proximity to BHQ-2 quencher; iv) 3MBP5 fluorescence remains quenched when the cells were incubated with M^{pro} and PL^{pro} inhibitors.